# Kinetic and metallographic study of the oxidation at high temperature of a cast Ni 25Cr alloy in water vapour-rich air

Lionel Aranda, Thierry Schweitzer, Ludovic Mouton, Sandrine Mathieu, Olivier Rouer, Pascal Villeger, Patrice Berthod, Elodie Conrath

# Kinetic and metallographic study of the oxidation at high temperature of a cast Ni 25Cr alloy in water vapour-rich air

Lionel Aranda[1], Ludovic Mouton[2], Sandrine Mathieu[2], Olivier Rouer[2], Pascal Villeger[1], Patrice Berthod[1,*] and Elodie Conrath[1]

[1]Institut Jean Lamour
Department N°2: Chemistry and Physic of Solids and Surfaces
Team "Surface and interface, chemical reactivity of materials"
[2]Common Service of Electronic Microscopy and Microanalysis
Faculty of Sciences and Technologies, University of Lorraine
B.P. 70239, 54506 Vandoeuvre-lès-Nancy – France

*E-mail Address: pberthodcentralelille1987@orange.fr

*Post-print version of the article* **Materials at High Temperatures 2015 VOL 32 N° 5 530–538.**

DOI 10.1179/1878641314Y.0000000041

**Abstract:** The high temperature oxidation behaviour of a Ni 25 wt.% Cr alloy in air enriched with water vapour (180 mbars $H_2O$) was studied at 1000, 1100, 1200 and 1300 °C. The oxidized samples were characterized by X-Ray diffraction, electron microscopy and wavelength dispersion spectroscopy. The obtained data were compared to the ones earlier obtained for the same alloy oxidized in dry air. Water vapour globally induced at all temperatures a decrease of the parabolic constant *Kp* and an increase of the chromia volatilization constant *Kv*. The oxide scales do not present morphologic difference between the two atmospheres. After oxidation in humidified air the scale thickness is thinner and the Cr-depleted depth is lower than in dry air.

**Keywords:** nickel-chromium alloy, high temperature oxidation, water vapour, thermogravimetry, kinetic parameters, metallographic characterization

## 1. Introduction

Superalloys are generally exposed to hot aggressive atmospheres when they are used in high temperature applications [1,2]. These atmospheres are often composed of air mixed with other oxidant gases as carbon oxides or water vapour notably [3,4]. Water vapour plays a particularly important role in the oxidation of the hottest pieces of jet engines. Gaseous water forms during kerosene combustion (several % of combustion gases) and this proportion may be increased when the propelled planes fly through clouds or over sea. Furthermore, water vapour is present in much higher proportion in the steam turbines used for power generation.

The presence of water vapour may influence the high temperature oxidation which occurs for blades despite the low partial pressure in oxygen. Its influence on hot oxidation, when present in air or in other gases, was examined in many

earlier studies. This was notably done in the cases of pure metals [5,6], intermetallic compounds [7,8], metallic coatings [9], alloys based on heavy refractory metals [10] and even ceramic materials [11].

Water vapour influences the progress of oxidation of alloys at high temperature by modifying the structural characteristics of the externally growing oxide scales. There are then consequences on the rates of mass gain or of mass loss [12]. Effects of water vapour were also found concerning the adherence of the external scale on the alloy substrate during isothermal oxidation [13] as well as when temperature varies [14, 15], notably in thermal cycling situation.

The chromium-rich superalloys which resist high temperature oxidation and corrosion by molten substances by developing an external continuous chromia scale are especially sensitive to the presence of water vapour. Their protective $Cr_2O_3$ scale can be affected, in water vapour-containing hot gases, by a re-oxidation [4] described by equation (1):

$$½\ Cr_2O_3\ (s) + H_2O(g) + ¾\ O_2(g) \rightarrow CrO_2(OH)_2(g) \qquad (1)$$

The oxy-hydroxides are volatile when temperature is high enough, but not so high as the 1000°C generally considered as required for the re-oxidation and volatilization of chromia (become gaseous $CrO_3$) in dry air. Several works showed that volatilization into gaseous $CrO_2(OH)_2$ may be significant at temperatures not higher than 600°C for binary [16] or commercial [17] iron-based chromia-forming alloys, for example. Such volatilization phenomenon induces, when the oxidation progress is followed by thermogravimetry, a decrease in mass gain rate leading to an underestimation of the oxidation kinetic. This is the reason why the treatment of the mass variations recorded by the thermobalance needs the separation of: on the one hand the parabolic contribution of the oxidation of the alloy, and on the other hand the linear mass loss due to chromia volatilization. Taking into account the linear mass loss by volatilization of chromia allows better characterizing the kinetic of high temperature oxidation of the alloy. Indeed, valuing the volatilization constant Kv allows avoiding to underestimate the parabolic constant Kp. Specifying simultaneously the real value of Kp and the linear constant Kv is thus very important. Such double determination can be done by treating the thermogravimetric results by applying in the present case a method which was previously established for the determination of the same constants in case of oxidation in dry air [18].

In this work it was wished to study the general kinetic of oxidation of chromia forming alloy in air enriched with water vapour at different levels of temperature, by performing thermogravimetry runs and by exploiting the obtained mass variations files according to the method described by equation (2) [18]:

$$m \times (dm / dt) = Kp - m \times Kv \qquad (2)$$

where m is the mass gain per surface unit area, t is time, Kp is the kinetic parabolic constant and Kv the kinetic linear constant which represents the rate of mass loss due to chromia volatilization.

The alloy taken in consideration for this work was a cast Ni (bal.) – 25 wt.% Cr one. It was chosen for its simple chemical composition (possible oxides: only of Cr and of Ni), its chromia forming behaviour existing up to very high temperature and its excellent resistance against local scale detachment due to growth-induced stresses. The goal was to compare the obtained kinetic constants, as well as the oxide characteristics of the oxidized samples, to the corresponding data obtained in parallel for the same alloy in dry air.

## 2. Experimental

### 2.1. The studied alloy

Four compact ingots (mass: about 40 g) were prepared by high frequency induction melting of pure nickel and pure chromium (Alfa Aesar, purity > 99.9 %) under inert atmosphere (300 mbars of pure Argon) in a CELES furnace (50 kW, operating parameters: 4 kV and 100 kHz). Two parallelepiped samples were prepared per test temperature: one for the test in humidified air and one for the test in dry air (for comparison). They were cut in each ingot (dimensions: about: 10 × 10 × 3 $mm^3$) by the mean of a Buehler Isomet 5000 precision saw. These samples were grinded all around with SiC papers from 240-grid to 1200 grid. Careful smoothing of their edges and corners was realized in order to avoid any risk of local catastrophic oxidation and to favour oxide adherence.

### 2.2. The thermogravimetry tests and their numerical treatment

All thermogravimetry tests were carried out with the same apparatus, a SETARAM SETSYS thermo-balance, coupled with a WETSYS vapour generator. Per ingot a sample was oxidized in “dry air” (industrial 80 % $N_2$ 20 % $O_2$, no water added) and another one was oxidized in “wet air” (industrial 80 % $N_2$ 20 % $O_2$ with addition of water). In the second case, water was introduced in air to achieve a partial pressure of 179 mbars. This was done by generating 90 % of relative humidity at 60 °C in the initial dry air before introduction in the thermobalance. The thermal cycle was composed of a heating with a rate of +20 °C $min^{-1}$, a {48 hours}-long isothermal stage at 1000, 1100, 1200 or 1300 °C, and a cooling with a rate of -5 °C $min^{-1}$.

The obtained thermogravimetry files were first visualized by plotting the mass gain versus time to control if the kinetic is globally parabolic. Second they were analysed by plotting the same data but according to equation (2) in order to value the two kinetic constants Kp and Kv. Plotting m × (dm / dt) versus -m effectively leads, for m become sufficiently important, to a straight line. The ordinate at origin of this one then led to Kp while its slope led to Kv.

### 2.3. Metallographic characterization of surfaces

The oxidized surfaces were first observed to get some qualitative data concerning the adherence of the oxide scale on the metallic samples (fraction of denuded alloy). Thereafter X-Ray Diffraction (Philips X’Pert Pro diffractometer; wavelength of the $K_\alpha$ transition of copper: $\lambda$ = 1.5406 Angströms) was carried out on the surface of the oxidized samples before cutting, to identify the nature of the oxide scales externally formed. Thereafter, the external scales were

subjected to carbon deposition and their general morphology was observed at high magnification, using scanning electron microscopy (Hitachi S4800 or JEOL JSM-7600F Field Emission Scanning Electron Microscopes).

2.4. Metallographic characterization in cross-section

The oxidized samples were coated all around with a thin gold layer using cathodic sputtering (Fine coater JEOL JFC 1200). This was done to allow thereafter the electrolytic deposition of a thick nickel layer in a heated Watts' bath, the role of which was protecting the oxide scale against possible degradation during cutting. The coated samples were cut in two parts using the Isomet 5000 precision saw. They were embedded in a cold resin mixture (ESCIL, araldite resin CY230 + hardener HY956), before being grinded with SiC papers from 120-grit to 1200-grit, ultrasonically cleaned, and polished again with 1µm paste to obtain a mirror-like surface state.

The oxide scales were observed in cross-section and their thickness measured, using a SEM (JEOL JSM6010LA). Their natures were confirmed by Energy Dispersion Spectrometry (EDS) using the EDS device equipping the SEM. Wavelength Dispersion Spectrometry profiles were performed across the alloy sub-surface to characterize the chromium-depleted zones: chromium content in the sub-surface close to the alloy/scale interface, and depth of Cr-impoverishment in the alloy.

## 3. Results

3.1. Thermogravimetry results

The four mass gain curves are presented together in Figure1. All are globally parabolic and the mass gain kinetic is logically faster for a higher stage temperature. These kinetics are all typical of a chromia-forming behaviour at each of these four temperatures. The curve form is not totally parabolic. For example the curve obtained at the lowest temperature (1000 °C) is a little irregular (affected by some oxide detachments). The one obtained at the highest temperature (1300 °C) presents an almost horizontal end part (obviously due to intense chromia volatilization).

By assuming that the Ni 25Cr oxidation progressed with chromia nucleation then growth, the mass gain data were treated according to equation (2). Two examples of such {m × (dm / dt) versus –m} plots are given in Fig. 2A (1100 °C) and Figure 3A (1300 °C). The four graphs effectively contained a linear part. A regression straight line was determined, the equation of which gave the value of Kp (ordinate at the origin) and Kv (slope). The obtained values are displayed in Table 1. The volatilization constant Kv logically increases with temperature, from about 50 to 640 × $10^{-10}$ g $cm^{-2}$ $s^{-1}$ between 1000 and 1300 °C. The parabolic constant Kp – thus corrected from the underestimation induced by chromia volatilization – also increases between 1000 and 1300 °C (3 to 230 × $10^{-12}$ $g^2$ . $cm^{-4}$ . $s^{-1}$). These values determined for Kp and Kv were thereafter verified by comparing, to the experimental mass gain curves, the model curves calculated using these Kp and Kv values. In all cases, the obtained {Kp, Kv} couples led to theoretic curves (called "math2" in the figures). They fit very well

the experimental curves (examples in Figure 2B for 1100 °C and Figure 3B for 1300 °C). There was not the case of the mathematical curves which would be obtained with classically determined Kp values (called “math1” in the figures).

The obvious dependence of the two constants on temperature was thereafter analysed by plotting the natural logarithm of these constants versus the reciprocal temperature (Arrhenius representation). This was done by considering the four temperatures for Kp but only the three highest ones for Kv. Indeed, the value of the volatilization constant obtained at 1000°C, curiously slightly higher than the one determined for the 100°C-higher temperature, is probably induced by the irregularities seen in Figure 1.

This led to points which are almost aligned, the regression straight lines of which allow proposing values for the activation energies: 237 kJ × $mol^{-1}$ for Kp and 241 kJ × $mol^{-1}$ for Kv. These values are very close to one another and are typical of a limitation of the oxidation kinetic by the diffusion of cationic vacancies.

### 3.2. Metallographic characterization of the oxidized surfaces

Preliminary observation of the oxidized surface showed that oxide scale spallation was more or less severe during the post-isothermal stage cooling. The surface fraction of denuded alloy increased with the temperature stage. For example, no significant loss of oxide was observed for the two samples cooled from 1000 °C while the denuded alloy surface fraction was the greatest for the two samples cooled from 1300 °C. In addition to the isothermal stage temperature it also appeared that humidity of air influenced the scale spallation during cooling. Indeed, for a given isothermal stage temperature, spallation was generally a little less severe in wet air than in dry air. These optical observations were confirmed by the analysis of the mass variation files during cooling (curves plotted versus temperature more or less irregular).

The SEM examination of the oxidized surfaces before cross-section preparation reveals that the average grain size of the chromia scale tends to increase with the oxidation temperature, as illustrated by the micrographs presented in Figure 6. The four oxidized samples were also subjected to X-ray diffraction runs. They all showed that chromia is the single oxide present on the sample surfaces, as illustrated in Figure 7 (sample oxidized at 1000 °C) and Figure 8 (1300 °C) for the two extreme temperatures. This confirms what was suggested by the mass gain and parabolic constants which were both typical of a chromia-forming behaviour. One can also notice in the diffractograms the presence of other peaks (noted “Ni”). These ones correspond to the austenitic nickel-based matrix of the alloy, appearing here and there on the surface of the samples where scale spallation during cooling led to zones of denuded alloy.

### 3.3. Metallographic characterization of cross-sections

After cross section preparation, the SEM examinations of oxide scales were realized through their thickness. Figure 9 presents SEM micrographs for the four oxidized samples. The oxide scale is exclusively made of chromia as verified by the homogeneous darkness of the whole thickness. This was confirmed by several EDS pinpoint measurements. A porosity state exists in the

chromia scales. The thickness of this scale logically increases with the isothermal stage temperature.

Two WDS concentration profiles were acquired in the subsurface, perpendicularly to the alloy/oxide interface. A profile per sample is shown in Figure 10 for example. The chromium content in the sub-surface close to the alloy/scale interface does not vary systematically versus the temperature of the isothermal stage. In contrast the alloy zone in which the chromium content had decreased during oxidation is obviously deeper for a higher temperature.

## 4. Discussion

The alloy under study here usually presents a very good behaviour in dry air for the same temperatures and for similar durations. The presence of a significant content of water vapour in air did not deteriorate this basis good behaviour (chromia-forming). The mass gains kinetic are fundamentally all of the parabolic type and if some of them are not exactly parabolic it is only due to chromia volatilization. The oxidation rates, considered by taking into account the more or less high temperature, are seemingly not considerably changed by comparison with oxidation in dry air. In addition the presence of water vapour seemed improving the resistance against oxide scale spallation during cooling. However some small differences may exist and it appeared interesting to directly compare the present kinetic and metallographic data to the corresponding ones obtained in a parallel work. This is done graphically thereafter.

The Kp and Kv values obtained in the present study (“WET”) and in a parallel work (“DRY”) are plotted together in Figure 11 (A: Kp, B: Kv) versus temperature. One can see that the parabolic constants issued from the {m × (dm / dt) = f(–m)} plots and treatments tend to be lower for oxidation in humidified air than in dry air. In contrast, the volatilization constants are rather close to one another for the lowest stage temperatures tested here. In contrast the value obtained for Kv at 1300 °C is significantly higher in humidified air than in dry air. The particularly high value of volatilization constant obtained at 1300 °C in the present work explains the apparent stationarity of the mass gain near the end of the isothermal stage (Figure 1).

Thus the presence of water vapour influenced the hot oxidation behaviour of the alloy. This concerned first the growth rate of the continuous external chromia scale, and second the rate of the loss of a part of this chromia oxide by volatilization. It also influenced the nature of the oxide scales since the ones covering the four samples of the present study were of pure chromia as demonstrated by XRD diffractograms. The presences of NiO and $NiCr_2O_4$ were in parallel additionally detected, by XRD measurements too, for the same alloy oxidized in dry air in the same conditions. In contrast the morphologies of the outer surface of the oxide scales formed in humidified air were not really different from the ones appeared on the parallel samples in dry air (illustrated by the SEM micrographs presented in Figure 12). This is in good agreement with previous results obtained about chromia scales formed in dry and wet atmospheres on binary Ni 25Cr alloys [19].

Additional differences between humidified air (this work) and dry air (parallel work) are highlighted in Figure 13 for the oxide scale thickness (A: significantly lower when formed in humidified air than in dry air) and for the Cr-depleted depth in the alloy subsurface (C: depletion depths lower for humidified air than for dry air). In contrast, no systematic difference was seen about the chromium content in the sub-surface close to the alloy / scale interface (B).

To summarize, the presence of water vapour with a partial pressure of about 180 mbars did not significantly transform the high temperature oxidation behaviour of the Ni 25Cr alloy by comparison with dry air, notably at the three lowest temperatures. However some differences were found, for example concerning the parabolic rate a little slower at all temperatures in wet air than in dry air. On the other hand the chromia volatilization was slightly enhanced at 1000 °C because air humidity, but the effect was much stronger at 1300 °C. At this latter temperature, the presence of water induced a significant acceleration of the volatilization of chromia. The effects of water vapour on the parabolic constant (which is lower in wet air than in dry air at 1100 and 1200 °C) and on the chromia volatilization constant (which is higher in wet air than in dry air at 1000 °C and at 1300 °C) contributed to the fact that the oxide scale thickness observed after oxidation in humidified air is lower than in dry air.

## 5. Conclusion

When the one-fifth of the atmospheric pressure is constituted by water vapour the general oxidation behaviour of this binary Ni 25Cr alloy is thus modified by comparison with its behaviour in dry air but not in great proportions. The modifications are, for some of them, a little detrimental. For example, more chromium initially belonging to the alloy is lost in gaseous species. But this is compensated by the better properties which are obviously brought to the external oxide scales by the fact that it grew in humidified air: nature exclusively chromia, lower diffusion of species through the scale as suggested by the lower values of Kp… Additionally the adherence of the scale on the alloy seems being better in humidified air than in dry air [14, 15]. Thus, the presence of water vapour in hot air seems being rather beneficial for the general oxidation behaviour of this alloy. This may be perhaps extrapolated to more complex chromia-forming refractory alloys and superalloys. However this remains to be verified but, in their cases, the possible oxidation of several metallic elements other than chromium risk to do not permit to follow the same procedure of {Kp, Kv} determination as used in the present work. Other means of chromia volatilization evaluation will be then used.

## 6. References

[1] Sims, C.T. (1972) Cobalt-Base Alloys. In: Sims, C.T. and Hagel, W.C. (eds), The Superalloys, pp. 150-174. John Wiley & Sons, New York.

[2] Donachie, M.J. and Donachie, S.J. (2002) Superalloys, A Technical Guide (2nd edition), ASM International, Materials Park.

[3] Kofstad, P. (1988) High Temperature Corrosion, Elsevier Applied Science, London.
[4] Young, D.J. (2008) High Temperature Oxidation and Corrosion of Metals (1st edition), Elsevier Corrosion Series, Amsterdam.
[5] Jonsson, T., Pujilaksono, B., Hallström, S., Agren, J., Svensson, J.E., Johansson, L.G., Halvarsson, M. An ESEM in situ investigation of the influence of $H_2O$ on iron oxidation at 500 °C. Corrosion Science, **51**, 1914-1924 (2009).
[6] Pérez, P. On the influence of water vapour on the oxidation behaviour of pure Ti. Corrosion Science, **49**, 1172-1185 (2007).
[7] Chevalier, S., Juzon, P., Przybylski, K., Larpin, J.P. Water vapor effect on high-temperature oxidation behavior of $Fe_3Al$ intermetallics. Science and Technology of Advanced Materials, art. n°045006, 10 (2009).
[8] Lin, Z.J., Li, M.S., Wang, J.Y., Zhou, Y.C. Influence of water vapor on the oxidation behavior of $Ti_3AlC_2$ and $Ti_2AlC$. Scripta Materialia, **58**, 29-32 (2008).
[9] Kaplin, C., Brochu, M. Effects of water vapor on high temperature oxidation of cryomilled NiCoCrAlY coatings in air and low-$SO_2$ environments. Surface and Coatings Technology, **205**, 4221-4227 (2011).
[10] Hellström, K., Tang, J.E., Jonsson, T., Halvarsson, M., Pompe, R., Sundberg, M., Svensson, J.E. Oxidation behaviour of a (Mo, W)Si2-based composite in dry and wet oxygen atmospheres in the temperature range 350-950 °C. Journal of the European Ceramic Society, **29**, 2105-2118 (2009).
[11] Yamauchi, A., Yi, X.M., Akiyama, T., Kurokawa, K. Oxidation Behavior of β-SiAlON in $H_2O$-Containing Atmosphere. Materials Science Forum, **696**, 395-399 (2011).
[12] Saunders, S. R. J., Monteiro, M., Rizzo, F. The oxidation behaviour of metals and alloys at high temperatures in atmospheres containing water vapour: A review. Progress in Materials Science, **53**, 775-837 (2008).
[13] Othman, N. K., Othman, N., Zhang, J., Young, D. J. Effects of water vapour on isothermal oxidation of chromia-forming alloys in $Ar/O_2$ and $Ar/H_2$ atmospheres. Corrosion Science, **51**, 3039-3049 (2009).
[14] Zurek, J., Young, D. J., Essuman, E., Hänsel, M., Penkalla, H. J., Niewolak, L., Quadakkers, W. J. Growth and adherence of chromia based surface scales on Ni-base alloys in high- and low-$pO_2$ gases. Materials Science and Engineering A, **477**, 259-278 (2008).
[15] Michalik, M., Hansel, M., Zurek, J., Singhheiser, L., Quadakkers, W. J. Effect of water vapour on growth and adherence of chromia scales formed on Cr in high and low $pO_2$-environments at 1000 and 1050°C. Materials at High Temperature, **22**, 213-221 (2005).
[16] Jonsson, T., Pujilaksono, B., Heidari, H., Liu, F., Svensson, J.-E., Halvarsson, M., Johansson, L.-G. Oxidation of Fe-10Cr in $O_2$ and in $O_2$+$H_2O$ environment at 600°C: A microstructural investigation. Corrosion Science, **75**, 326-336 (2013).
[17] Halvarsson, M., Tang, J. E., Asterman, H., Svensson, J.-E., Johansson, L.-G. Microstructural investigation of the breakdown of the protective oxide

scale on a 304 steel in the presence of oxygen and water vapour at 600°C. Corrosion Science, **48**, 2014-2035 (2006).
[18] Berthod, P. Kinetics of high temperature oxidation and chromia volatilization for a binary Ni–Cr alloy. Oxidation of Metals, **64(3/4)**, 235-252 (2005).
[19] Essuman, E., Meier, G. H., Zurek, J., Hänsel, M., Norby, T., Singheiser, L., Quadakkers, W. J. Protective and non-protective scale formation of NiCr alloys in water vapour containing high- and low-$pO_2$ gases. Corrosion Science, **50**, 1753-1760 (2008).

## TABLES

Table 1
Values of the kinetic constants derived from the {m × (dm / dt) = f(-m)} plot of the thermogravimetric results

| Temperature | Kp ($\times 10^{-12}$ $g^2 . cm^{-4} . s^{-1}$) | Kv ($\times 10^{-10}$ $g . cm^{-2} . s^{-1}$) |
|---|---|---|
| 1300 °C | 230 | 643 |
| 1200 °C | 34.5 | 103 |
| 1100 °C | 7.04 | 42.6 |
| 1000 °C | 3.21 | 48.7 |

Table 2
Values of the thickness of the external oxide scales (in µm)

| Temperature | average | standard deviation |
|---|---|---|
| 1300 °C | 30.8 | 5.0 |
| 1200 °C | 11.7 | 1.5 |
| 1100 °C | 6.8 | 0.9 |
| 1000 °C | 5.8 | 2.5 |

Table 3
Values of the chromium content in extreme surface (in wt.%)

| Temperature | average | standard deviation |
|---|---|---|
| 1300 °C | 19.4 | 0.3 |
| 1200 °C | 17.9 | 1.9 |
| 1100 °C | 19.9 | 0.5 |
| 1000 °C | 18.3 | 0.8 |

Table 4
Values of the depth of the Cr-depleted zone (in µm)

| Temperature | average | standard deviation |
|---|---|---|
| 1300 °C | 455 | 43 |
| 1200 °C | 197 | 7 |
| 1100 °C | 96 | 7 |
| 1000 °C | 40 | 4 |

## FIGURES

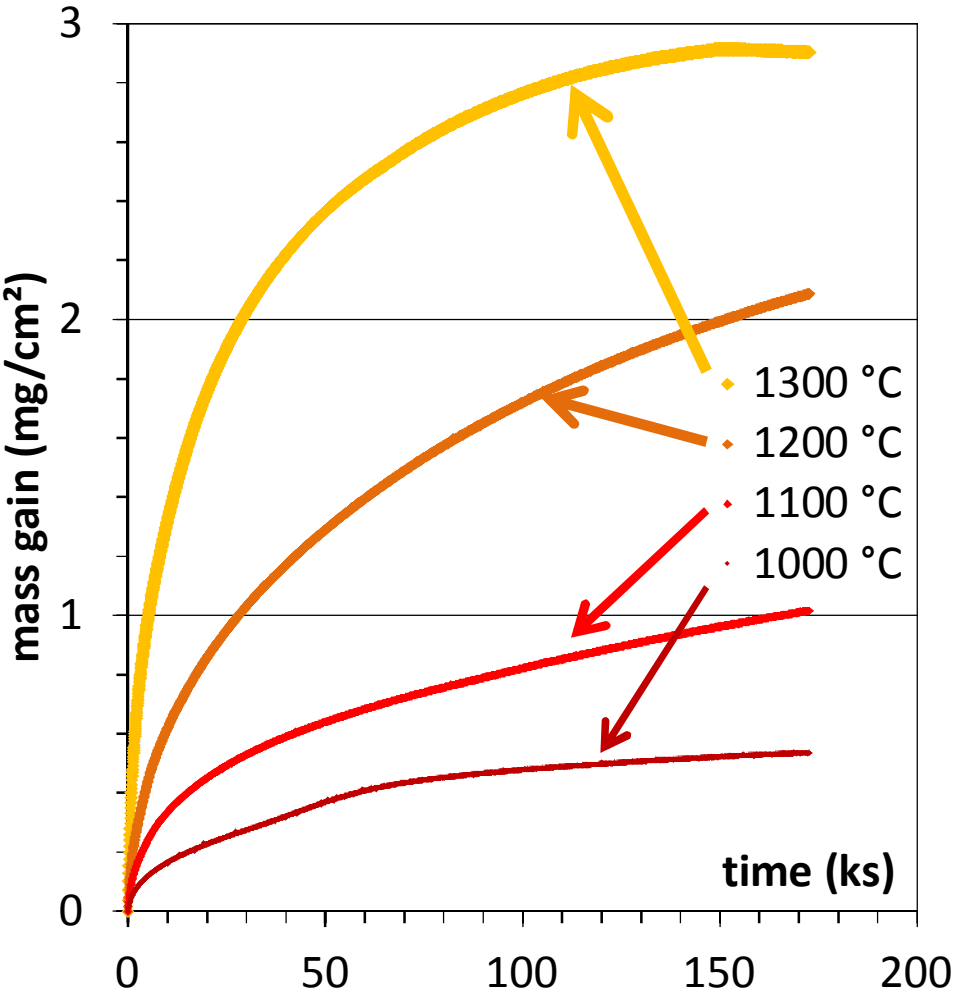


Fig. 1. The thermogravimetry curves obtained for the four temperatures of oxidation of the Ni 25Cr alloy in wet air

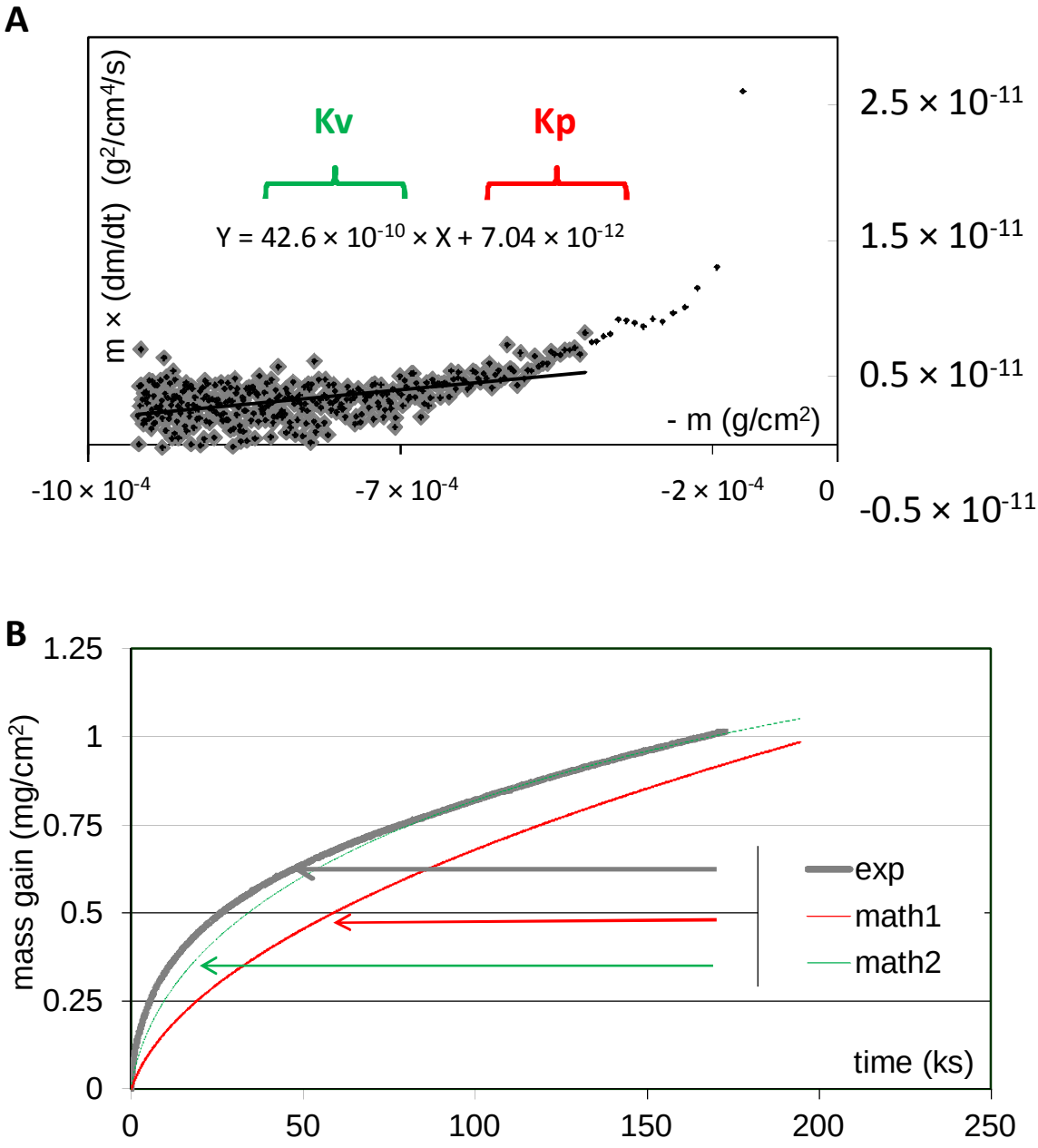


Fig. 2. Example of the thermogravimetry results at 1100 °C: {m × (dm / dt) = f(-m)} plot of the mass gain records (**A**) for the determination of the constants Kp and Kv; test of the conventionally obtained Kp constant and of the {Kp, Kv} couple of constants values issued from the {m × (dm / dt) = f(-m)} plot

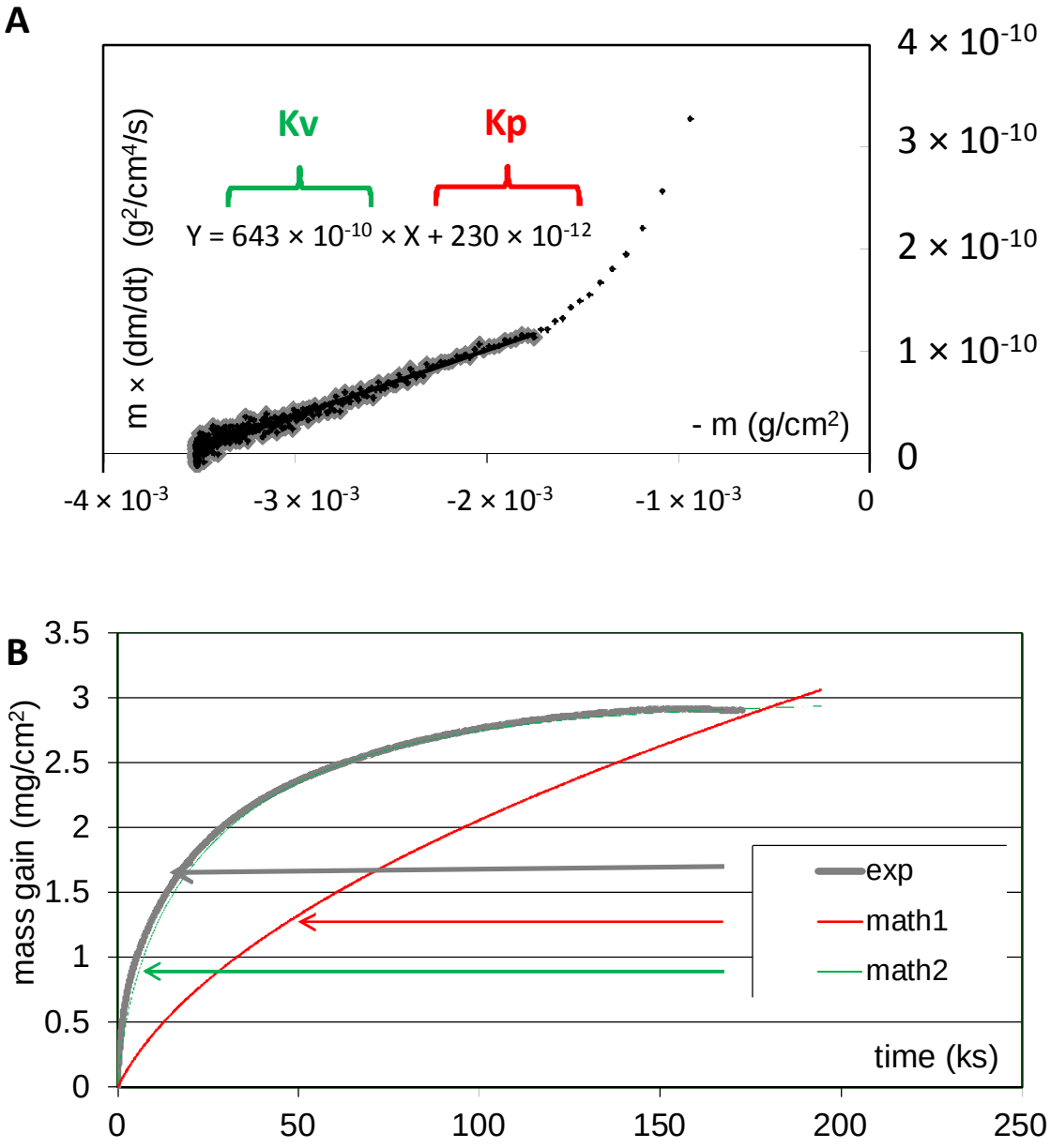


Fig. 3. Example of the thermogravimetry results at 1300°C: {m × (dm / dt) = f(-m)} plot of the mass gain records (**A**) for the determination of the constants Kp and Kv; test of the conventionally obtained Kp constant and of the {Kp, Kv} couple of constants values issued from the {m × (dm / dt) = f(-m)} plot

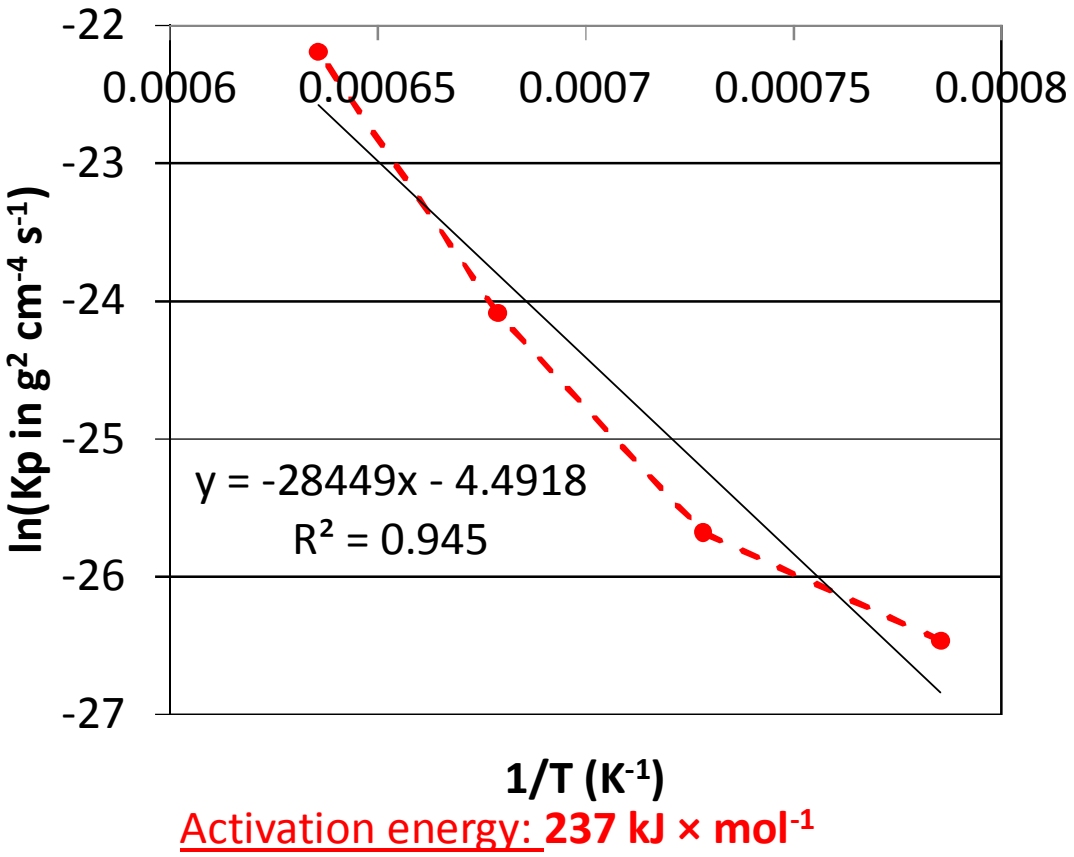


Fig. 4. Arrhenius plot of the parabolic constant Kp (issued from the {m × (dm / dt) = f(-m)} plot); determination of the activation energy

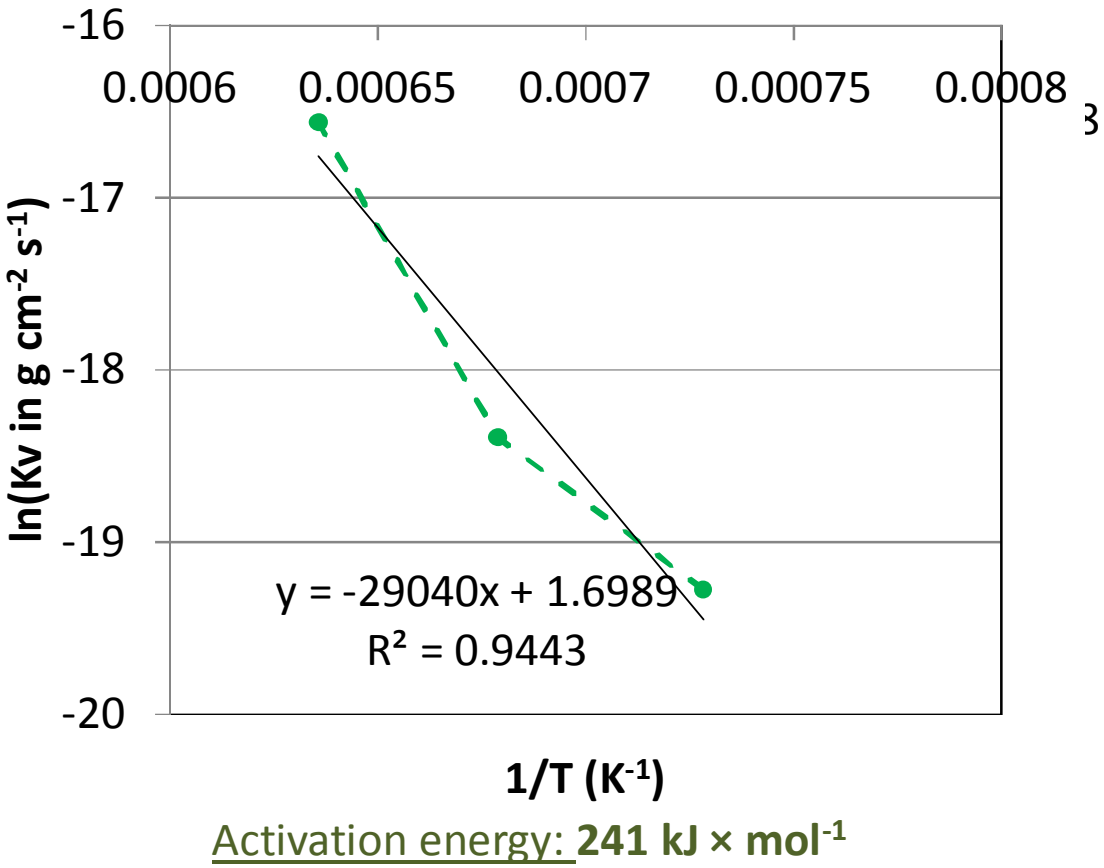


Fig. 5. Arrhenius plot of the parabolic constant Kv (issued from the {m × (dm / dt) = f(-m)} plot); determination of the activation energy

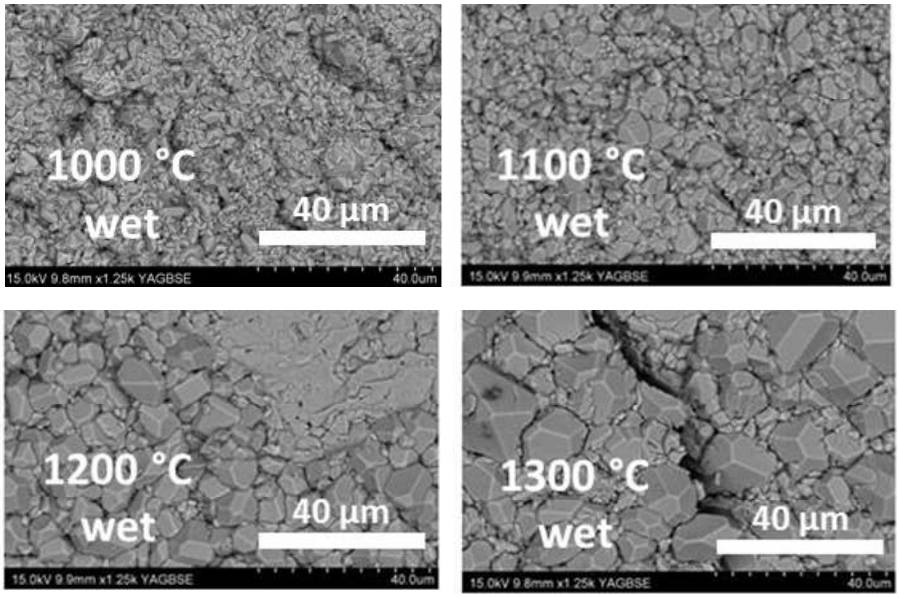


. 6. SEM micrographs of the external oxide scale formed over the four samples

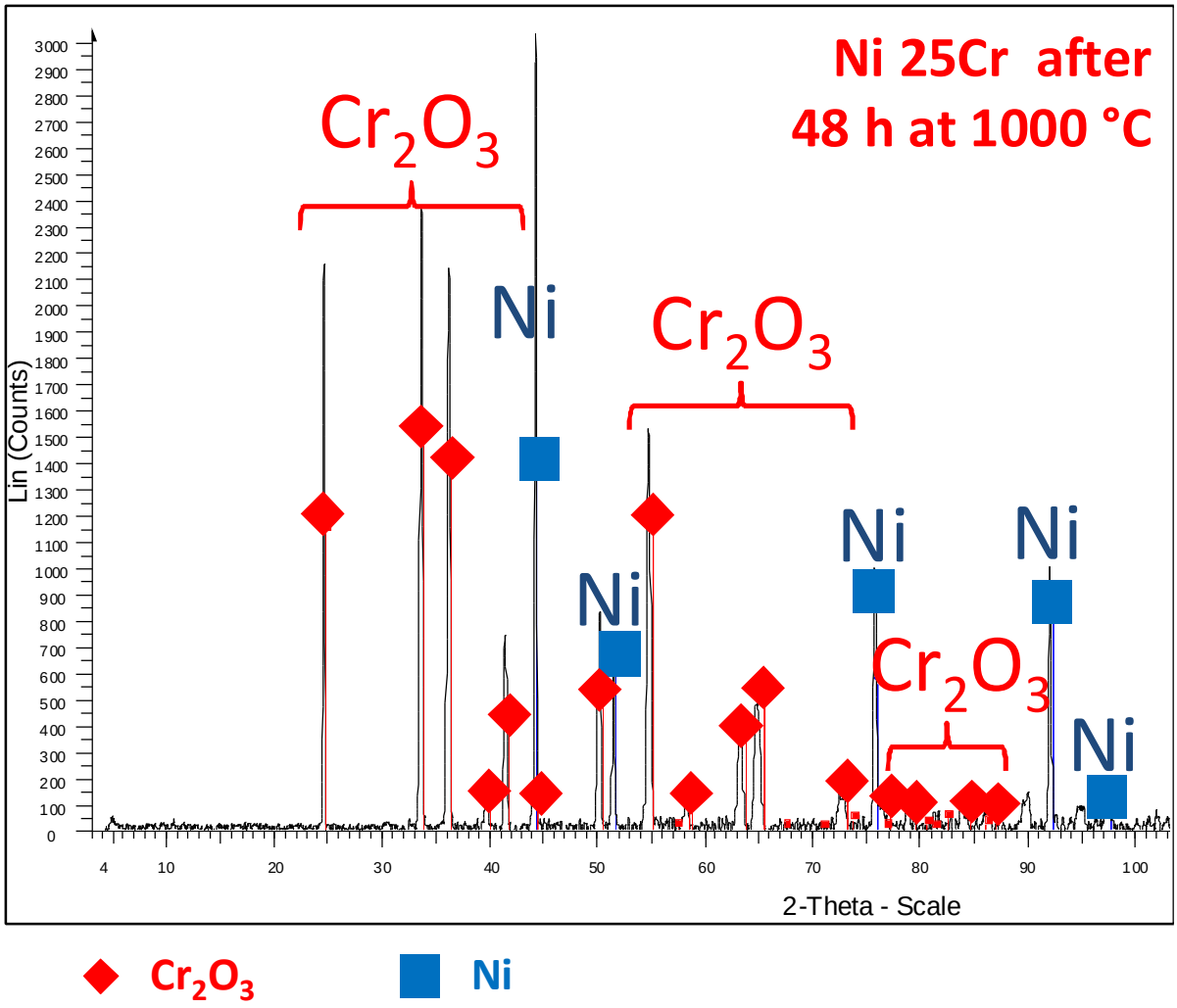


Fig. 7. Diffractogram obtained for the external oxide scale formed over the sample oxidized at 1000 °C

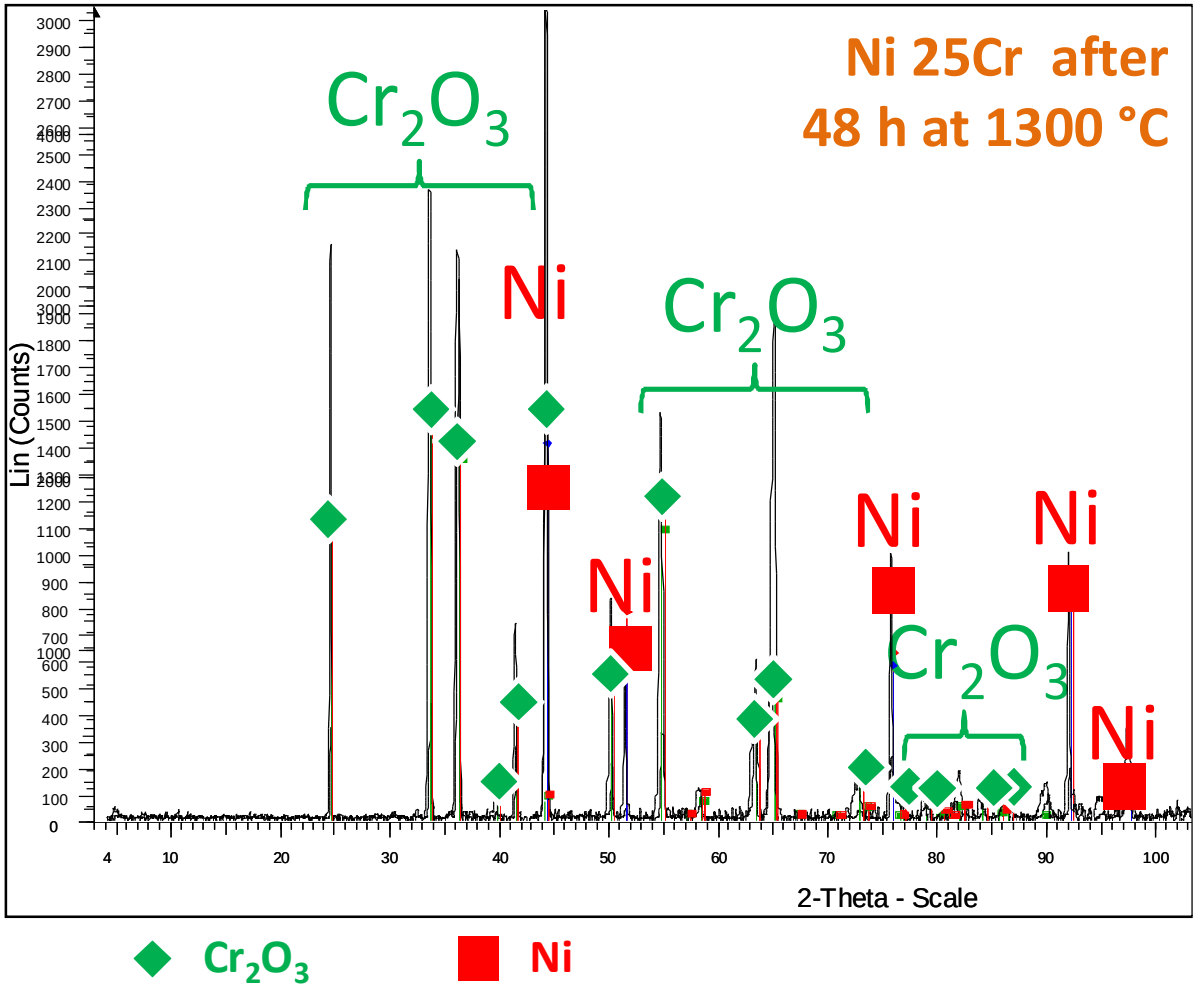


Fig. 8. Diffractogram obtained for the external oxide scale formed over the sample oxidized at 1300 °C

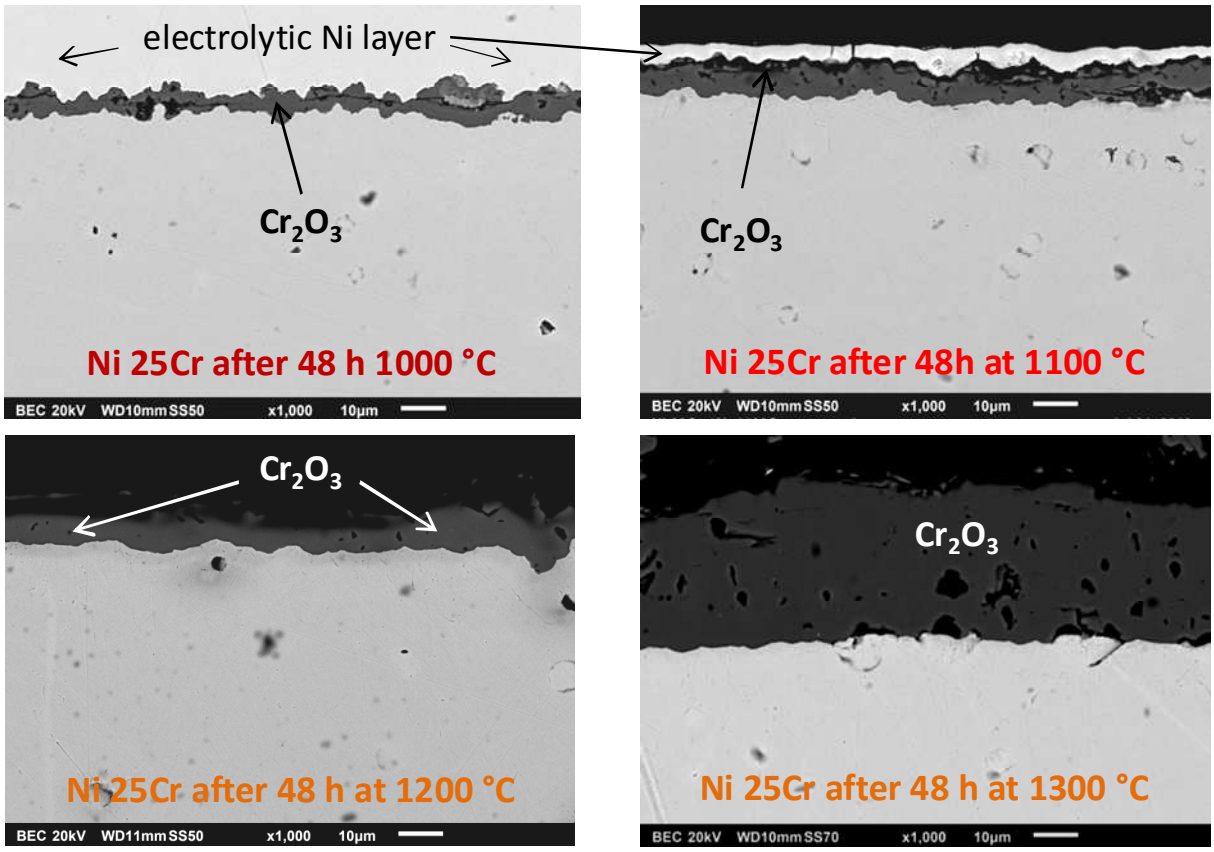


Fig. 9. Cross sections of the four oxidized samples (SEM.BSE micrographs)

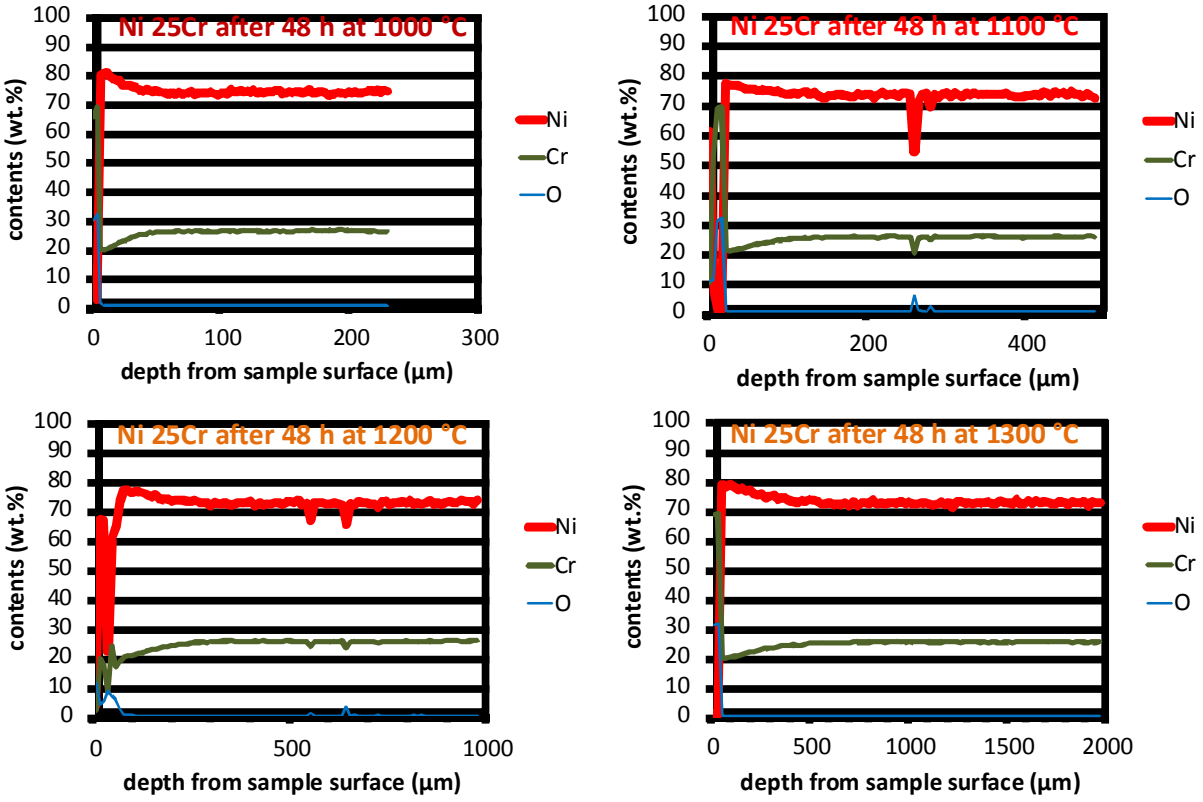


Fig. 10. Concentration profiles acquired through the Cr-depleted zones of the four oxidized samples

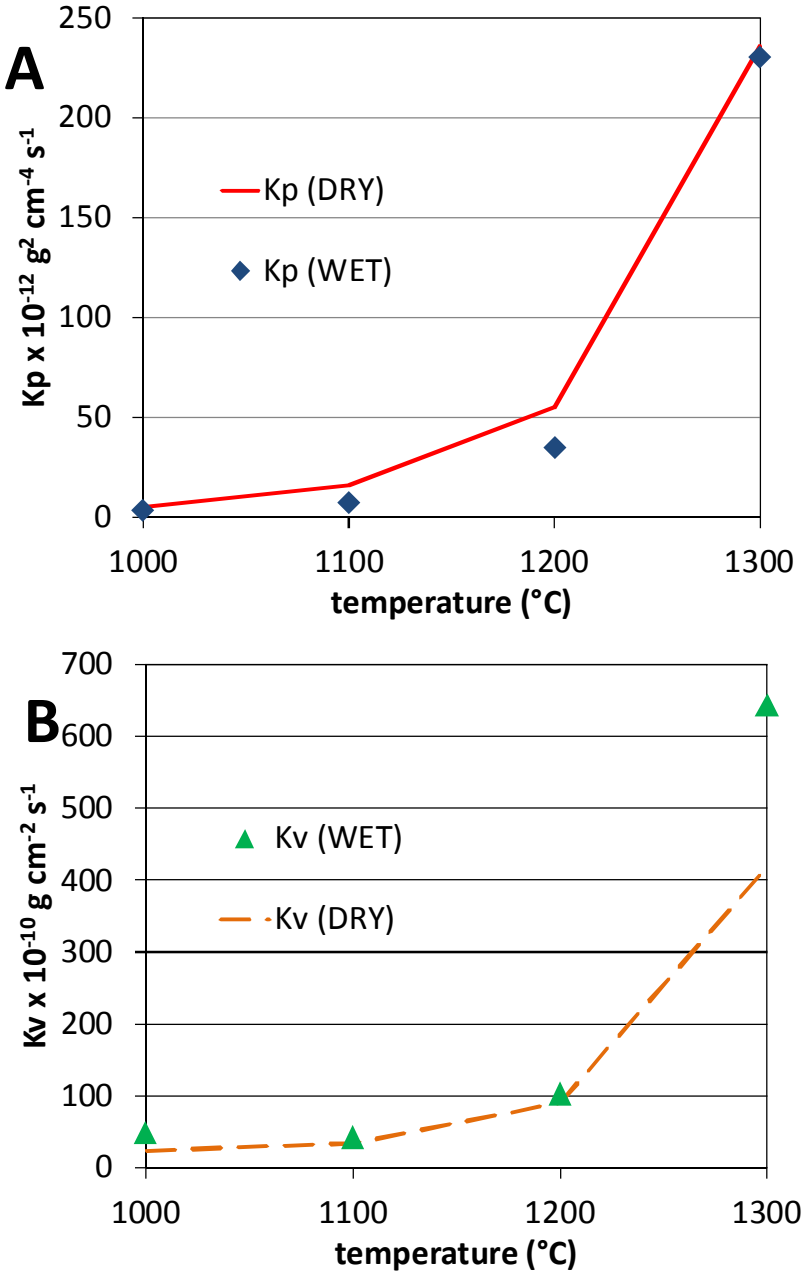


Fig. 11. Comparison of the kinetic constants of the Ni 25Cr alloy at the four temperatures between wet air and dry air (**A**: Kp, **B**: Kv)

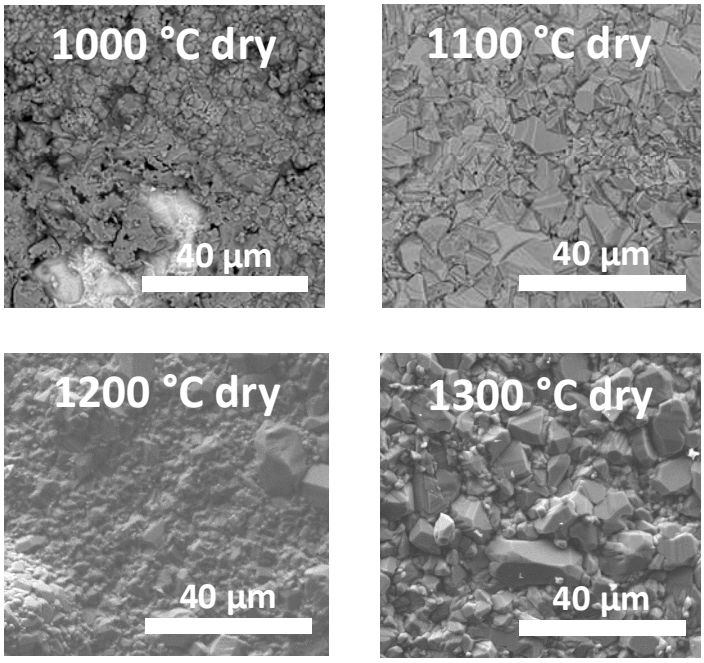


Fig. 12. SEM micrographs of the outer oxide scales formed over the Ni 25Cr samples in dry air during 48 h at the four temperatures

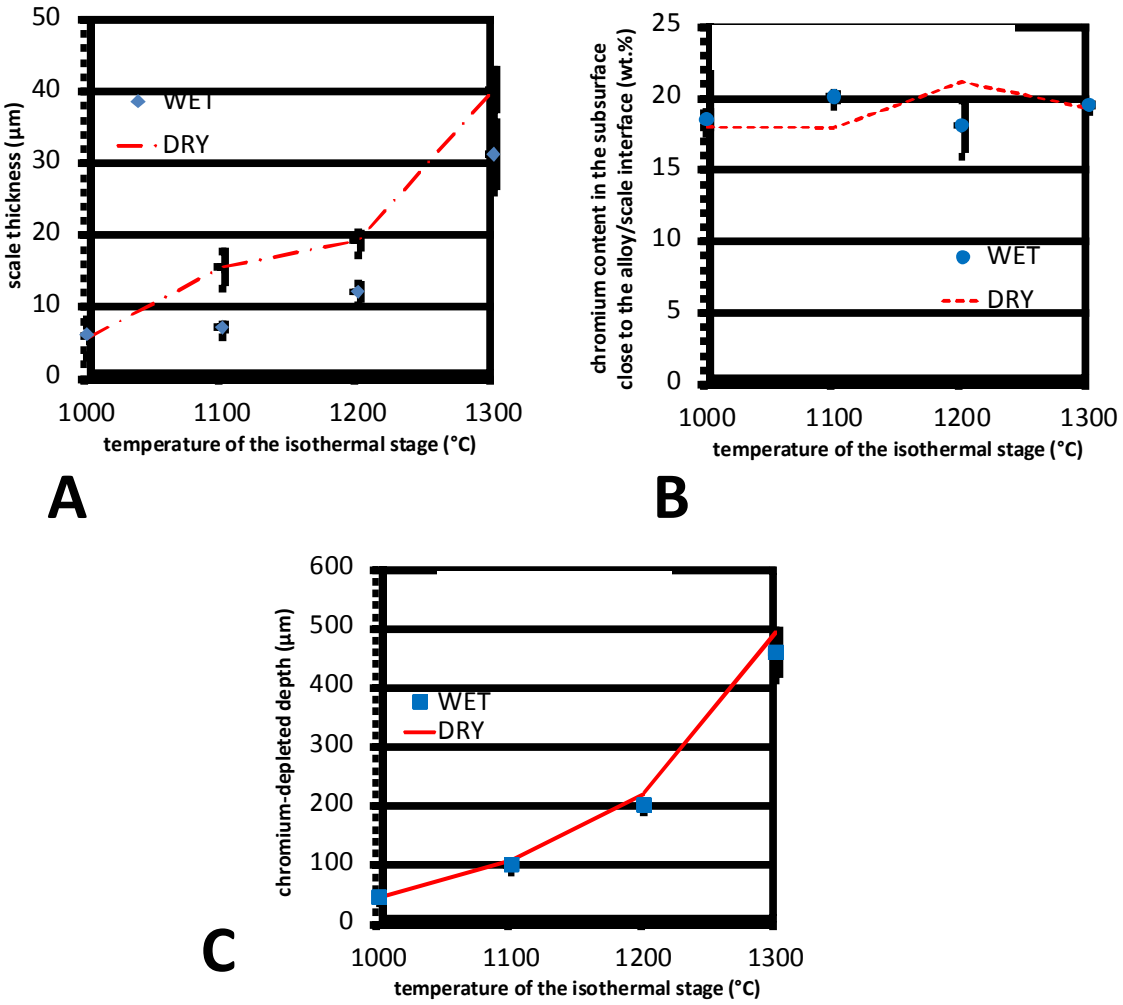


Fig. 13. Comparison of the scales' thicknesses (**A**), the alloy chromium contents in extreme surface (**B**) and the Cr-depleted depths (**C**) of the Ni 25Cr alloy at the four temperatures between wet air and dry air